

Flares observed with XMM-Newton and the VLA

Kester Smith^{1*}, Manuel Güdel², and Marc Audard³

¹ MPIfR, Auf dem Hügel 69, 53121 Bonn, Germany

² Paul Scherrer Institut, Würenlingen und Villigen, CH-5232 Villigen PSI, Switzerland.

³ Columbia Astrophysics Laboratory, Columbia University, 550 West 120th Street, New York, NY 10027, USA

kester@mpifr-bonn.mpg.de

guedel@astro.phys.ethz.ch

audard@astro.columbia.edu

Received 22nd September 2004, ; Accepted 16th December 2004

Abstract. We present lightcurves obtained in X-ray by the *XMM-Newton* EPIC cameras and simultaneous radio lightcurves obtained with the VLA for five active M-type flare stars. A number of flare events were observed, and by comparing radio with X-ray data, we consider various possible flare mechanisms. In cases where there seems to be a clear correlation between radio and X-ray activity, we use an energy budget argument to show that the heating which leads to the X-ray emission could be due to the same particles emitting in the radio. In cases where there is radio activity without corresponding X-ray activity, we argue that the radio emission is likely to arise from coherent processes involving comparatively few particles. In one case, we are able to show from polarization of the radio emission that this is almost certainly the case. Cases for which X-ray activity is seen without corresponding radio activity are more difficult to explain. We suggest that the heating particles may be accelerated to very high energy, and the resulting synchrotron radio emission may be beamed in directions other than the line of sight.

Key words. Stars: late-type – stars: coroneae – stars: flare

1. Introduction

Convection and differential rotation in late-type stars combine to drive a magnetic dynamo, leading to the formation of a corona. The solar corona is readily observable due to the Sun's proximity. In the case of other stars, magnetic activity may manifest itself through various chromospheric emission lines, quiescent soft X-ray and microwave emission, and the occurrence of flaring behaviour. Stars with rapid rotation, either due to a young age or membership of close binary systems, display much more extreme coronal activity than the Sun. Numerous small flares are the leading candidate for the main mechanism of coronal heating on the Sun (Krucker & Benz 1998), and there is growing evidence that the same mechanism could be responsible for coronal heating in other, more magnetically active stars (e.g. Audard et al. 2000, Kashyap et al. 2002, Güdel et al. 2002b, Güdel et al. 2003, Audard et al. 2003).

Standard models of solar flares envisage the key process to be acceleration of electrons and ions by magnetic reconnection (see e.g. Benz 2002). The energy in the electron (or ion) beam then gives rise to the flare emis-

sion. Three main emission mechanisms can be identified. First, radio gyrosynchrotron emission from the magnetically confined electrons, which accounts for a small fraction of the energy. Second, hard X-ray emission which is produced as the electron beams collide with the chromosphere, and which also accounts for a small portion of the energy. Third, soft X-ray emission is produced from evaporating chromospheric material heated to around 10^7 K (Dennis 1988). This accounts usually for the bulk of the emitted energy. There is, therefore, a physical relationship between the radio gyrosynchrotron emission and the X-ray emission, which, on the Sun, manifests itself in various observable effects for individual flares. Temporal and spatial correlations between components of individual flare events can be investigated to build up a detailed picture of the flaring process. For flare stars, however, spatial information is not available, and temporal resolution is heavily compromised by the need for integration times sufficient to yield acceptable signal-to-noise ratios. We must therefore search for coarser relationships between different emission types, which can point to similarities with or differences to the solar models. An indication that radio emission and soft X-ray emission are generally linked comes from the relation between the quiescent radio emission and X-ray luminosities, which holds over a wide range of flare ener-

Send offprint requests to: K. Smith

* Present address: STScI, 3700 San Martin Drive, Baltimore MD 21218, USA

gies from different types of flaring object (Güdel & Benz 1993). Temporal relations can also sometimes be observed. For example, the Neupert effect, in which the soft X-ray flux is proportional to the integrated radio flux, is evidence that heating of and evaporation from the chromosphere is driven by the same population of fast particles which gives rise to the radio emission (Neupert 1968, Dennis & Zarro 1993). Examples of the Neupert effect in stellar sources include Güdel et al. (1996), for UV Cet and recent observations of σ Geminorum (Güdel et al. 2002a) and Proxima Centauri (Güdel et al. 2002b).

The new generation of X-ray satellites, offering greatly enhanced sensitivity in the soft X-ray regime, makes it easier to pursue simultaneous radio and X-ray monitoring programmes aimed at flare stars, with a view to searching for temporal correlations between radio and X-ray activity. In this paper we present a collection of time series observations for five active stars, all of which are M dwarfs. In each case, we have combined VLA radio observations with simultaneous *XMM-Newton* EPIC observations, to search for any relationship between the gyrosynchrotron radio and soft X-ray emission.

2. Target objects

The five targets discussed in this paper are all active late-type stars known to show strong coronal activity. AD Leo is an dM3.5e star of apparent magnitude $V=9.43$ lying at a Hipparcos distance of approximately 4.7 pc. It shows an apparent rotation period of 2.7 days (Spiesman & Hawley 1986) and $v \sin i$ of 5 km s^{-1} (Vogt, Penrod & Soderblom 1983) which together suggest a high inclination between the stellar rotation axis and the plane of the sky ($\sim 75^\circ$). The system is in fact binary, with a very low mass infrared companion at a separation of 78 mas, or 0.366 AU (Balega, Bonneau & Foy 1984). The quiescent and flaring X-ray emission were studied by Favata et al. (2000) who used a combination of *Einstein*, ROSAT and ASCA data and drew conclusions about the nature of magnetic structures in the flaring corona. Stepanov et al. (2001) observed an intense radio flare from the star, which was interpreted as coherent emission from a flare loop. Güdel et al. (2003) studied the statistical flaring properties of AD Leo, fitting power laws to the flare energy distribution to investigate the possibility of coronal heating being caused by small flares. Hawley et al. (1995, 2003) conducted a multi-wavelength study of flaring behaviour, combining observations from ground based optical observatories, HST STIS spectroscopy, EUVE data, as well as microwave observations from MERLIN. They observed several examples of a Neupert effect between the EUVE soft X-rays and the U-band emission, which is a proxy for hard X-ray emission. Van den Besselaar et al. (2003) presented *XMM-Newton* and Chandra spectra of AD Leo (and also showed the *XMM-Newton* lightcurve presented here), and derived various properties of the corona, including the possible presence of an inverse FIP effect.

AU Mic is an active dM0e dwarf at a distance of 10pc with a rotation period of 4.85 days (Vogt et al 1983). It forms a distance and proper motion pair with AT Mic, although the two are separated by 1.5° on the sky. Detailed modelling of the hydrogen spectrum by Houdebine & Doyle (1994) revealed many of the conditions prevailing in the chromosphere and transition region. Microflaring on timescales of seconds was detected in U-band photometry by Andrews (1989). X-ray variability was studied by Ambruster et al. (1987). Kundu et al. (1987) observed AU Mic, and also AT Mic, at microwave frequencies with the VLA. A massive flare was observed by EUVE on this object in July 1992, and is discussed by various authors, including Cully et al. (1994) who modelled the slow decay phase as being due to the ejection of a magnetically confined plasmoid, an event similar to a solar coronal mass ejection. The time-varying UV spectral lines during this event were discussed by Monsignori Fossi et al. (1996) and also by Katsova et al. (1999). The quiescent UV spectrum was studied by Pagano et al. (2000), who derived an emission measure distribution and compared the conditions to those on the Sun. FUV flare behaviour was studied by Robinson et al. (2001) using HST spectra.

AT Mic is a dM4.5e+dM4.5e binary with an apparent separation of $3''.5$ at a distance of 10.2 pc. UV and optical flaring behaviour was described by Bromage et al. (1986), and simultaneous optical, infrared and microwave observations were made by Nelson et al. (1986). The microwave spectrum was studied by Large et al. (1989) who concluded that two components were present, variable emission from a coherent process producing a falling spectrum below about 1 GHz, and a probable gyrosynchrotron process producing a flat spectrum. Gunn et al. (1994) saw a blue shifted component in the profile of the Ca II H and K lines during a flare, which they interpreted as evidence of chromospheric evaporation. X-ray spectra of AT Mic obtained by *XMM-Newton* and Chandra were presented by Raassen et al (2003). This paper also presented the EPIC pn lightcurve analysed here.

UV Cet is a dM5.5e+dM4.5e binary at a distance of 2.7 pc. The projected separation on the sky is about $2''$. Radio observations have shown significant differences in the behaviour of the two stars, despite their similar basic properties. The quiescent primary is much weaker than the secondary, and often produces highly polarized flares, suggesting a coherent emission mechanism. The secondary flares more frequently, but produces only moderately polarized flares suggestive of a gyrosynchrotron origin. VLBA observations of UV Ceti B show that the radio source is extended to about 4 – 5 stellar radii. This is thought to indicate trapping of accelerated particles in large coronal loops. The primary was found to be pointlike in these observations. The two components were recently distinguished in X-rays for the first time by Audard et al. (2003). They found that the quasi-steady X-ray behaviour of the two components was similar, in contrast to the quiescent radio emission. The apparent quiescent emission of component B was probably composed of numerous small

Table 1. Summary of the target objects and observations log. The final column lists the duration of the simultaneous observation, i.e. the length of time over which both X-ray and radio data were obtained. In the case of UV Cet, this duration is identical for the 5 GHz and 8.3 GHz data

Source	Spectral Type	d (pc)	P (d)	Observing date	Simultaneous observation length (ks)
AD Leo	dM3.5e	4.7	2.7	14.05.2001	31.54
AU Mic	dM0e	10	4.85	13.10.2000	20.74
AT Mic	dM4.5e+dM4.5e	10.2		15.10.2000	16.16
UV Cet	dM5.5e+dM5.5e	2.7		07.07.2001	30.24
YZ CMi	dM4.5e	5.9		09.10.2000	20.04

flares. The brighter radio emission of UV Cet B may be due to more effective trapping of accelerated particles in the large coronal loops of this object.

YZ CMi is a dM4.5e star at a distance of approximately 5.9 pc. UV observations by Robinson et al. (1999) revealed flaring activity on a range of time and energy scales. VLBI observations by Pestalozzi et al. (2000) resolved the corona at 3.6 cm to extend $1.77 \times 10^{10} \pm 8.8 \times 10^9$ cm, or $0.7 \pm 0.3 R_*$ above the photosphere.

3. Observations

The X-ray data are from the *XMM-Newton* guaranteed time programme. The X-ray lightcurves were constructed using standard techniques with *SAS*, and were smoothed by using a Savitzky-Golay smoothing algorithm (as implemented in IDL). The smoothing employed here uses in each case an 11-point 4th-degree kernel. The Savitzky-Golay filter provides an estimate of the first derivative of the curve, which is of interest when considering possible correlated X-ray and radio events. The X-ray hardness ratio was also measured. We defined this as the hard count rate, in a band between 1.5 and 4.5 keV, divided by the soft count rate, in the band 0.3 to 1.5 keV.

The VLA observations were scheduled to be simultaneous with the *XMM-Newton* X-ray observations. Most of the observations were carried out in October 2000, with the VLA in C configuration. All the radio observations for AD Leo, AU Mic, AT Mic and YZ CMi were made at 6 cm. UV Cet was observed at both 6 cm (5 GHz) and 3.6 cm (8.3 GHz). The low frequency band was chosen for most of the observations primarily because the flare gyrosynchrotron emission is expected to exhibit a falling spectrum, so that the detection likelihood for marginal events is maximised. The need to observe phase calibrators introduced gaps into the time coverage. Typically, the target would be observed for approximately three to four minutes, and then a calibrator would be observed for approximately two minutes. The data were reduced using standard tasks in AIPS. The integration time was ten seconds, which is then the minimum available binning time in the data reduction. Lightcurves were produced by coherently averaging the real and imaginary parts of the visibility on a timescale of typically one scan, before finally determining the stellar flux. The radio data could

be rebinned at higher resolution to closely study a few interesting events.

The observations and basic data for the target objects are summarized in Table 1.

4. Overview of the analysis

We pay particular interest to time correlations between X-ray and radio events. Approximately simultaneous X-ray and radio events suggest the possibility of the Neupert effect. The correlation arises because the gyrosynchrotron (radio) emission is proportional to the instantaneous number of fast particles, whilst the slowly variable soft X-ray emission is roughly proportional to the accumulated total energy. Thus,

$$L_R(t) \propto \frac{d}{dt} L_X(t), \quad (1)$$

where L_R and L_X are the radio and soft X-ray luminosities. It is for this reason that the first derivative of the X-ray lightcurve is of interest. If flaring behaviour in radio is correlated quite closely with the gradient of the X-ray lightcurve, this then provides an *a priori* implication that the Neupert effect may be occurring in a given flare. This hypothesis is impossible to prove, but for each case where we suspect it is present, we carry out a plausibility analysis based on the energy budget. The energy of the radio-emitting particles can be estimated from the radio flux, with various assumptions, and this can be compared to the X-ray energy actually measured. If the Neupert effect hypothesis is accepted, this also places a constraint on the possible combination of magnetic field strength and electron power-law index. We outline the argument in some detail below (Sect. 4.1).

If radio events occur which have no X-ray counterpart, the most likely explanation is that the observed microwave flux arises from some process with low intrinsic energy in the electrons, most probably an electron-cyclotron maser. Such emission is expected to be highly circularly polarized. From the observing frequency, the local magnetic field strength can be estimated.

Cases in which an X-ray flare is observed to have no discernable radio counterpart are more problematic to explain. Some form of heating process must be occurring, but any emission from accelerated particles is somehow hidden

from our view. Radio synchrotron emission from very high energy particles is highly anisotropic and is predominantly directed perpendicular to the field, $\eta_\nu \propto \sin\theta^{(\delta+1)/2}$, where η_ν is the emissivity, δ is the power-law slope of the electron distribution, and θ is the angle between the line of sight and the local magnetic field (Dulk 1985). In the case of low energy electrons, the emission is directed parallel to the field, with $\eta_\nu \propto \cos\theta^2$ for the fundamental, and in the intermediate case of gyrosynchrotron emission from mildly relativistic particles, the emission is broadly peaked perpendicular to the field ($\eta_\nu \propto \sin\theta^{-0.43+0.65\delta}$). The apparent absence of radio emission accompanying some X-ray flares may point to the heating particles being unusually low or unusually high in energy, with an appropriate field geometry.

4.1. Kinetic energy budget for radio flares

We follow here the analysis laid out in detail in Güdel et al (2002a) for a flare event of σ Geminorum. In outline, we first estimate the number of accelerated particles produced and the total energy contained in the distribution, based on the radio flux observed, then compare this to the energy radiated in X-rays. A number of assumptions must be adopted in making the estimate of the available kinetic energy.

Non-thermal electrons in solar and stellar flares typically have a power law energy distribution,

$$n(E, t) = \frac{N(t)(\delta - 1)}{E_0} (E/E_0)^{-\delta}, \quad (2)$$

where $N(t)$ is the instantaneous number density of electrons of all energies and E_0 is a cutoff energy for the distribution of non-thermal electrons, which we chose to set at 10 keV, a value probably lower than typical solar flares which have $E_0 \sim 10 - 20$ keV (Dennis 1988). We assume, based on solar analogy that the power law index lies in the range $2.0 < \delta \leq 3.5$ and $E_0 = 10$ keV (see Dennis 1988). The total instantaneous kinetic energy of the distribution is then

$$E_{kin} = N(t)V(t) \frac{\delta - 1}{\delta - 2} E_0, \quad (3)$$

where $N(t)$ is the number density of electrons with energy above E_0 , and $V(t)$ is the source volume. If the source were optically thin, the observed radio flux over all bands would be,

$$f_R(t) = \frac{\eta V(t)}{d^2}, \quad (4)$$

where η is the emissivity. In practice, we observe the radio flux in a narrow band at 5 GHz (or 8.3 GHz in the case of UV Cet). Furthermore, the emission will probably not be entirely optically thin. We correct for this by using some assumptions about the usual nature of stellar coronal spectra. In many flares, the turnover from optically thick low frequencies to optically thin high frequencies occurs around 10-20 GHz, although can be as low as a few GHz

(Morris et al. 1990). The spectral index is typically +1 on the optically thick low frequency side and between -0.5 and -1 on the optically thin high frequency side. We can therefore estimate that at 5 GHz the intrinsic radio emission is in the region of 1 - 10 times that observed. We assume a factor of 5 in the estimates which follow, which corresponds to assuming the peak frequency $\nu_{peak} \sim 10$, and spectral indices of +1 and -1 for the optically thick and optically thin sides respectively.

The gyrosynchrotron emissivity for the X-mode is given by

$$\eta_x = 3.3 \times 10^{-24} 10^{-0.52\delta} B N(t) (\sin\theta)^{-0.43+0.65\delta} \times \left(\frac{\nu}{\nu_B} \right)^{1.22-0.9\delta}, \quad (5)$$

where B is the magnetic field and ν_B is the electron gyrofrequency (Dulk & Marsh 1982). In what follows, we routinely consider values of B between 20 and 200 G and set θ , the viewing angle, to 60° , since most of the emission arises from electrons with large pitch angles. We further assume the O-mode emissivity is roughly equal to the X-mode emissivity, so that $\eta \approx 2\eta_x$.

As a flare evolves, the number of accelerated particles is incremented by ongoing acceleration processes, whilst the existing population decays with some timescale τ . Thus

$$\frac{d[N(t)V(t)]}{dt} = \frac{d[N_+(t)V(t)]}{dt} - \frac{N(t)V(t)}{\tau}, \quad (6)$$

where N_+ is the total number of particles added by acceleration. This equation may be integrated in time twice over the duration of the flare to obtain the total number of injected electrons. If, after the flare, the number of additional particles returns to preflare levels, (which can be judged to be the case if the flux returns to preflare levels) the first term on the right hand side will not contribute to the integral and the total number of injected electrons is

$$N_{tot} = \frac{1}{\tau} \int_{T_0}^T N(t)V(t) dt. \quad (7)$$

Combining equations 4, 5 and 7 we obtain

$$N_{tot} = 1.55 \times 10^{19} 10^{3.49\delta} B^{0.22-0.9\delta} \frac{d^2}{\tau} \int_{T_0}^T f_R(t) dt. \quad (8)$$

An appropriate value for the timescale τ is estimated from the observed radio variations during the event. In practice, we have usually adopted half the decay time for the radio flare, unless shorter timescale variations are evident during the decay phase. Equation 3 can then be used to determine the available energy.

5. Results and discussion

5.1. AD Leo

The *XMM-Newton* EPIC pn and VLA 5 GHz lightcurves are shown in Figure 1, together with the X-ray hardness

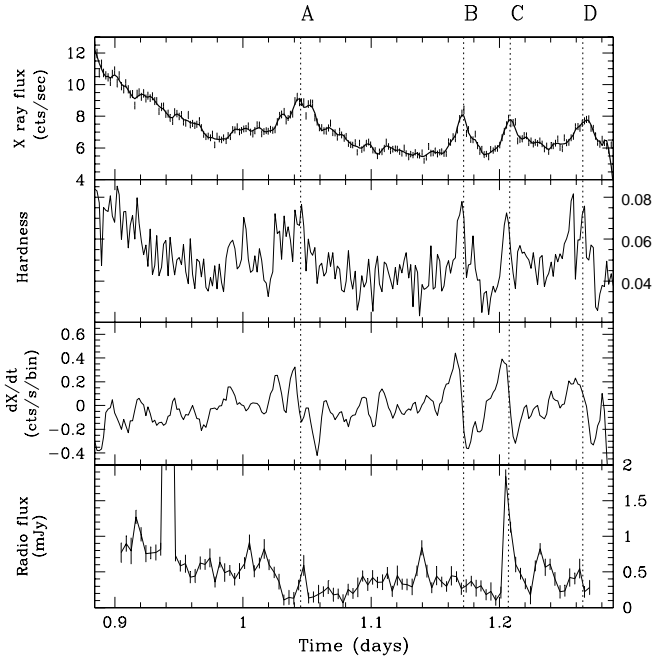


Fig. 1. Lightcurves for AD Leo. From top: EPIC lightcurve, flare hardness ratio, time derivative of the X-ray lightcurve, and radio lightcurve at 5 GHz. The time axis is labelled in days after IAT midnight on 14.05.2001 (IAT differs from UT by the addition of 32 seconds). The identified X-ray flares are marked with dotted lines and labelled at the top of the plot.

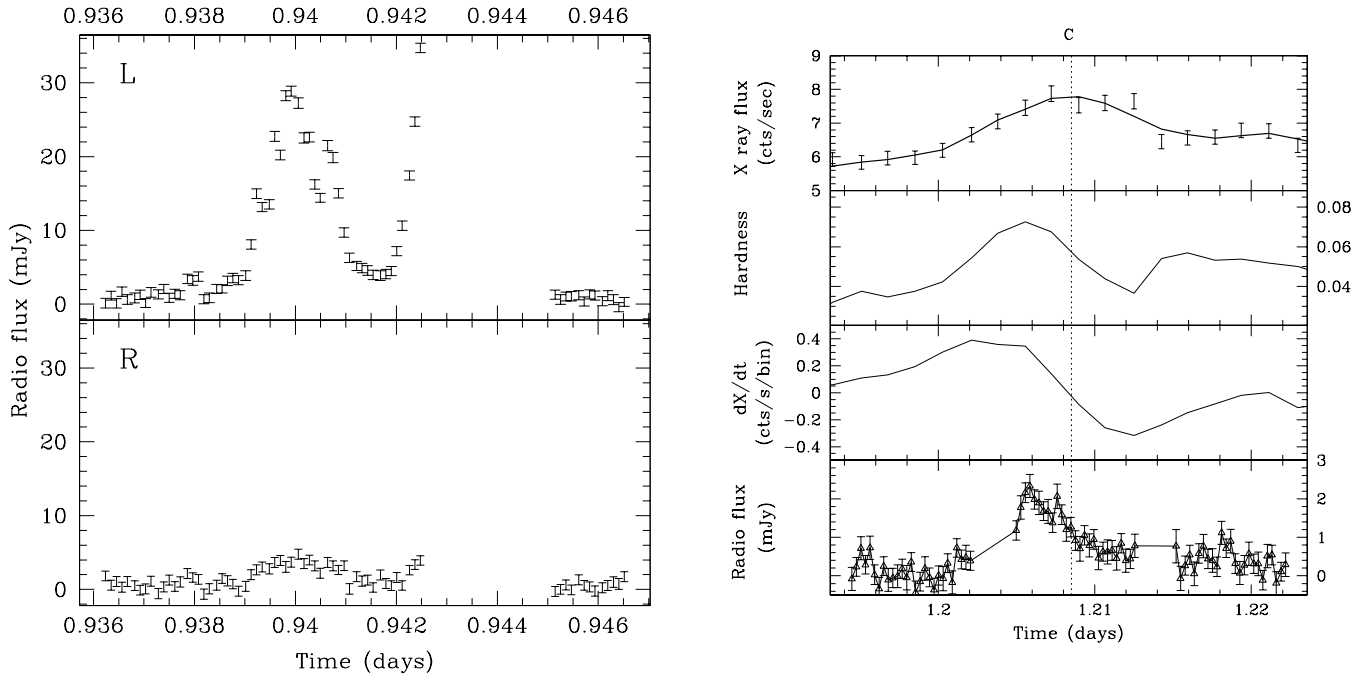


Fig. 2. Left: Closeup of the radio lightcurve for the first radio event. The top panel shows the L flux, and the lower panel the R flux. The gap is the break between scans, during which time the phase calibrator was observed. Right: Closeup of the event at 1.2 days (event C), showing the relative timing of the X-ray flux, derivative of X-ray flux and radio flux.

ratio and the first derivative of the X-ray lightcurve. The top panel shows the *XMM-Newton* pn lightcurve, and a

smoothed version of this made using a Savitzky-Golay smoothing algorithm. The second panel shows the X-ray

hardness ratio for the flare. The third panel shows an estimate of the time derivative of the X-ray lightcurve, also obtained using the Savitzky-Golay filter. The bottom panel shows the radio lightcurve at 6cm.

Four distinct bright X-ray flares can be observed in the EPIC lightcurve (Fig 1), and have been labelled A,B,C and D for ease of reference. Additionally, the beginning of the lightcurve shows the decay phase of an earlier large outburst. Apparently continuous low-level radio activity is present from the beginning of the VLA observation up to approximately 1.02 days. A large, shortlived radio flare occurs at around 0.94 days, and has no clear counterpart in the X-ray lightcurve. This flare is truncated on the scale in the lower panel of Figure 1. In the left hand panel of Figure 2 we show a higher time resolution plot of the radio lightcurve at the time of this early radio flare. The left-hand circularly polarized (LCP) flux is shown in the top panel, and the right-hand polarized (RCP) in the lower panel. This radio flare is almost 100% left-hand circularly polarized, suggesting that this is a coherent emission process requiring fewer accelerated particles and apparently leading to negligible chromospheric heating. The main candidates for the emission process are either an electron cyclotron maser, arising from a population of relativistic electrons trapped in a magnetic flux tube, or plasma maser emission. The former hypothesis allows us to directly estimate the magnetic field strength in the emitting region, provided we assume the emission occurs at the fundamental gyrofrequency

$$\nu_c = \frac{eB}{2\pi m_e c} \approx 2.8 \times 10^6 B. \quad (9)$$

For our observations (6 cm \equiv 5 GHz), this implies $B \sim 1.8$ kG. This would drop by a factor of two if the emission in fact occurred at the first overtone. Plasma maser emission would occur at the fundamental plasma frequency

$$\nu_p = \left(\frac{n_e e^2}{\pi m_e} \right)^{\frac{1}{2}} \approx 9000 n_e^{0.5}, \quad (10)$$

which then implies that the density of the emitting material would be $\sim 3 \times 10^{11}$ cm $^{-3}$, which is higher than values typically found for stellar coronae, but not dramatically so. Applying the energy budget argument laid out in Sect. 4, for the value of the magnetic field suggested above, the available kinetic energy of the accelerated particles is found to be of order 10^{29} erg, one or two orders of magnitude less than the radiated energy of most observed X-ray flares (see below).

A time-symmetric X-ray brightening occurs at about 1.04 hours (event A). The early part of this feature occurs whilst the radio flux is enhanced, apparently by a succession of modest flares, in the early part of the lightcurve (up to about UT=1.03 days). A small radio flare occurs at around the time of the peak of event A.

To estimate the total energy emitted in the X-ray event, we have used a standard Raymond-Smith model for a thermal plasma, with parameters typical of M dwarfs

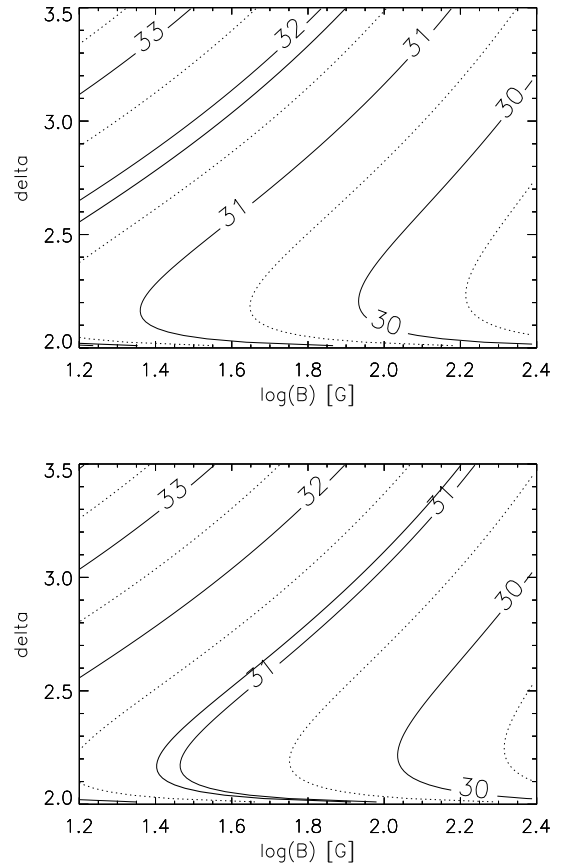


Fig. 3. Top: Estimated kinetic energy of the emitting particles in the AD Leo flare at T=1.05 days (event A) as a function of δ and B . The solid contours show values of $\log(\text{energy})$. Half decades are shown with dotted lines. The contour corresponding to the estimated radiated X-ray energy (approximately 7×10^{31} erg) is marked with a bold solid line. Bottom: The equivalent plot for event C.

($kT=1$ keV, $n_{abs} \sim 10^{18}$ cm $^{-2}$), to estimate the mean energy per photon. We estimate from the observed count rate that around 7×10^{31} erg are radiated in the X-ray flare. The available energy from the accelerated particles estimated from the radio flux as described above in Section 4.1 is plotted as a function of B and δ in Figure 3 (upper panel). The radiated X-ray energy accounts for a high fraction of the available energy, even with helpful assumed values of B and δ . Also, although the small flare at T=1.05 days is simultaneous with the peak of the X-ray flare, the brightening in X-rays is sustained over a much longer timescale, so that the radio activity does not correlate very closely with the overall X-ray behaviour. It therefore seems likely that the total radio flux associated with the heating particles is not visible to us. One way this might occur is if the radio emission is strongly anisotropic, as discussed above in Section 4. Strongly anisotropic emission is expected for synchrotron emission from very high energy particles, and the flux would be mostly directed

perpendicular to the field lines. The lack of a radio counterpart to event A would then imply that the field loops lie approximately along the line of sight for most of their length.

A small radio flare occurs at around $T=1.14$ days. This radio flare was found not to be significantly polarized. Nevertheless, there is no X-ray counterpart.

Event B, at $UT=1.17$ days, has no clear radio counterpart in the overall lightcurve. A closer examination of the radio lightcurve at higher time resolution revealed no significant short timescale brightening at this time, although there were low-level fluctuations in the lightcurve greater than the noise level. None of the small peaks exceeded 1 mJy in brightness. The radiated X-ray energy is approximately 2×10^{31} erg. It seems highly unlikely that this energy is provided by particles whose radio emission we observe. Anisotropic emission seems a more likely explanation.

The third radio flare is approximately simultaneous with the third X-ray flare, event C (Figure 2, right hand panel). The close-up shows that the X-ray lightcurve in fact peaks some 4 minutes after the radio peak. The gradient of the X-ray lightcurve correlates well with the radio emission. As noted above, this correlation is expected from the Neupert effect. We again follow the steps outlined in Sect. 4.1 to assess the plausibility of the Neupert effect hypothesis. We used values of δ between 2.0 and 3.5 and B between 20 and 200 Gauss. The decay timescale is estimated from the radio lightcurve to be around 180 s. A contour plot of energy as a function of these parameters is shown in Figure 3. The total injected energy is between 10^{29} erg and 10^{33} erg. Just over 10^{31} erg is emitted in the X-ray flare. The Neupert effect hypothesis is therefore broadly consistent with the energy budget in this case. However, the radio flare was found to be strongly left-hand circularly polarized ($\sim 75\%$). This implies that a large fraction of the radio emission arises from processes other than gyrosynchrotron. If we assume that the observed emission is a blend of gyrosynchrotron emission, with a 20% polarization, and emission from some coherent process, which is nearly 100% polarized, this would mean that about 30% of the total emission would be gyrosynchrotron. There would still be sufficient energy in this case to allow for the observed X-ray flux.

Radio activity occurring just after event C, at about $T=1.24$ days, had no clear X-ray counterpart and was also left-hand circularly polarized at the 50-100% level. This is therefore most likely emission due to some coherent process.

A final X-ray variation occurs near the end of the observation (event D). The total energy radiated in X-rays is approximately 1.4×10^{31} erg. The radio lightcurve is not particularly well-correlated but does show some brightening at this time.

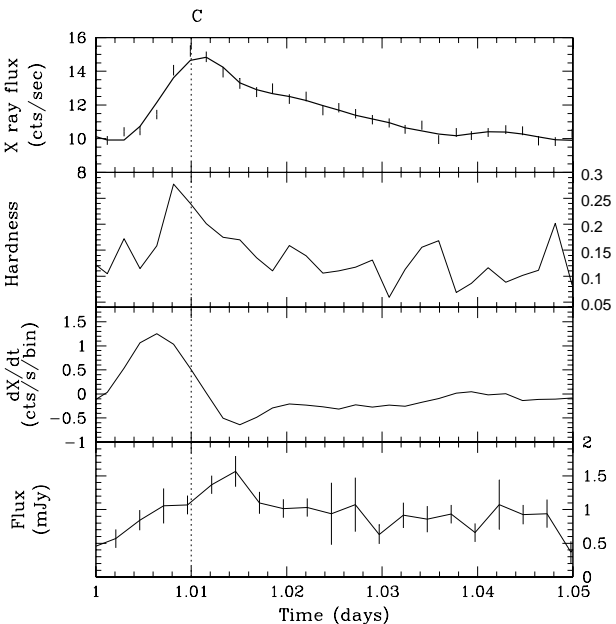
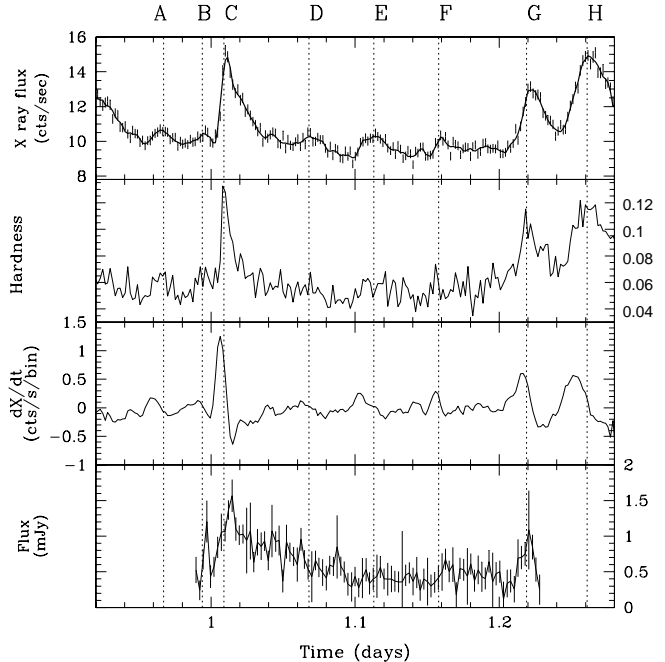


Fig. 4. Upper figure, from top to bottom: X-ray flux, hardness ratio, derivative of X-ray flux and radio flux for AU Mic. The time axis is labelled in days since IAT midnight on 13.10.2000. Lower figure: close up of lightcurves around event C.

5.2. AU Mic

The *XMM-Newton* pn and VLA 5GHz lightcurves are shown in Figure 4, together with the hardness ratio and X-ray lightcurve derivative. We have labelled eight distinct events in the X-ray lightcurve with letters A-H. Event A occurs before the radio lightcurve begins, and event B oc-

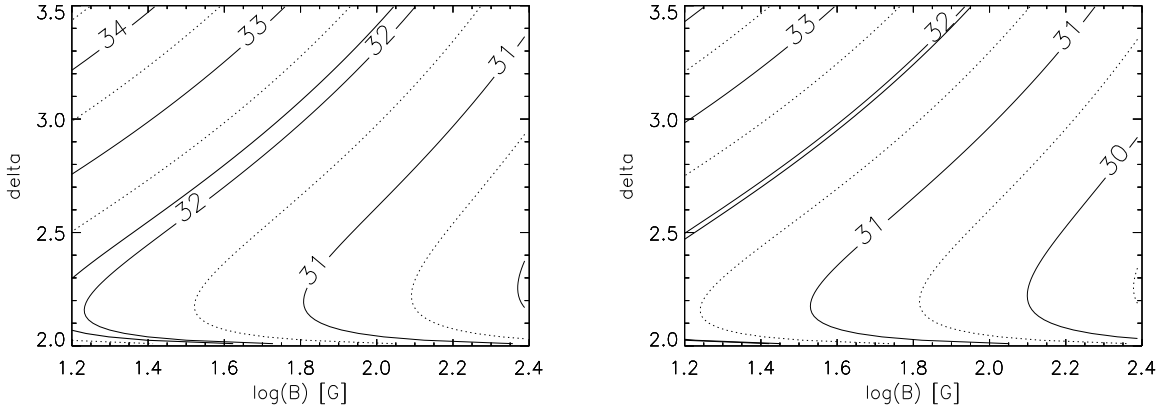


Fig. 5. Estimated kinetic energy of the emitting particles in the AU Mic radio flares corresponding to X-ray flares C (on the left) and G (on the right) as functions of δ and B . The solid contours show values of $\log(\text{energy})$. Half decades are shown with dotted lines. The bold solid lines show the radiated X-ray energy. This was approximately 1.5×10^{32} erg for event C and 9×10^{31} erg for event G.

curs only slightly after the onset of the radio lightcurve. Nevertheless a sharp spike in the radio lightcurve occurs at about this time.

Event C seems to be correlated with the large radio flare at the beginning of the radio lightcurve. This section of the lightcurve is shown in greater detail in the lower panel of Figure 4. This first radio flare is assumed to last from the beginning of the observation until $t = 1.03$ days, when the radio emission dips temporarily, although it could be argued that the decay phase in the radio lasts much longer, until around UT=1.15 d. Following the same argument used for AD Leo above, with an estimated decay timescale τ , of 500 s corresponding to the most rapid timescale seen in the flare, at around 1.025 days, we estimate the energy available at the flare site to be between 10^{30} and 10^{34} erg (see Figure 5, left hand panel). The radiated X-ray energy is estimated to be 1.5×10^{32} erg (see Fig. 6 left-hand panel).

A further small X-ray event, labelled D, occurs late in the decay phase of the radio flare and has no clear radio counterpart. Two further small events in the X-ray lightcurve, E and F, have no clear radio signature, although F may correspond to a slow increase in radio flux at about this time. A larger flare at the end of the radio data, event G, has a clear radio counterpart. Here, the total available energy is approximately 10^{30} – 10^{33} erg, while the X-ray event radiates approximately 9×10^{31} erg. The kinetic energy of the accelerated particles is plotted as a function of B and δ in the right-hand panel of Figure 5. The X-ray energy needed is at the high end of the range of available energies estimated from the radio lightcurve. A larger X-ray flare, labelled H, occurs after the end of the radio lightcurve. None of the radio variations showed a level of circular polarization above approximately 20%.

5.3. AT Mic

Although the binary components of AT Mic could be distinguished in the VLA maps, it is difficult to produce separate lightcurves because the VLA beam is highly distorted over short intervals. We have therefore considered the total flux of both objects together. The lightcurves are shown in Figure 6. The radio flux increased at the beginning of the observation, reaching a plateau of around 1.5 mJy, and then showed signs of a decrease towards the end of the observation. There was little or no rapid activity in the radio lightcurve once the plateau was reached. The flux was approximately 30% LCP throughout.

We have identified three events in the X-ray lightcurve (labelled A, B and C). A and B each show an unusual profile with a flat top and approximately equal rise and decay phases, although event B is much stronger than event A. Event C is a very gentle time symmetric brightening which occurs after the radio observation had ended and will not be discussed further.

The energy radiated in X-rays by event A is estimated to be approximately 1.5×10^{32} erg. The energy radiated by event B is approximately 6×10^{32} erg. No short-timescale radio counterpart could be found for either event.

5.4. UV Ceti

The components of UV Ceti were not distinguishable in the X-ray frames. For this star, we obtained radio data at both 5 and 8.3 GHz. These are shown separately in Fig. 7. The X-ray lightcurve shows almost continuous flaring activity. To avoid confusion, we have labelled only two events in the figure, which are somewhat larger and more distinct than the others and which correspond roughly in time to radio activity. The radio lightcurves also show what may be a continuous sequence of small flares. The lightcurves at the two different radio frequencies are very similar, except for the large flare near the end of the observations, which

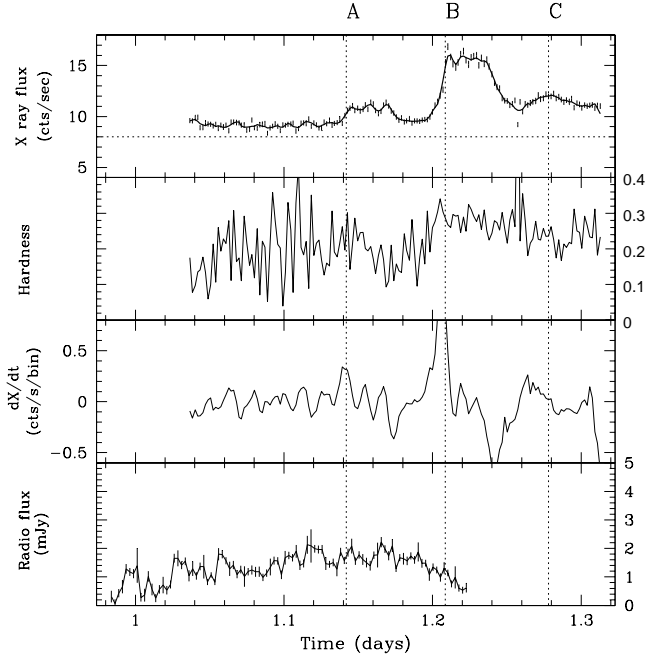


Fig. 6. AT Mic lightcurves. From top to bottom, X-ray flux, hardness ratio, derivative of X-ray flux, and radio flux. The time axis is labelled in days since IAT midnight on 15.10.2000.

is seen strongly at 5 GHz and hardly appears at all at 8.3 GHz.

Event A occurs just after the beginning of the radio observations. A small radio flare occurs shortly afterwards at 8.3 GHz, and a few minutes later a small flare is seen at 5 GHz. The X-ray flare radiates just over 1×10^{30} ergs. This is in the middle of the range of available energy as a function of B and δ as estimated from either radio band. However, the correlation between the radio flux and the derivative of the X-ray lightcurve is highly questionable (Fig. 8 upper panel).

Event B corresponds well to a local peak in the lightcurve at 8.3 GHz, and precedes the larger flare seen at 5 GHz by several minutes (see Fig. 8, lower panel). The radiated X-ray energy is around 10^{30} erg, which lies approximately in the mid range of available energies estimated from the 8.3 GHz radio flux and towards the low end of energies available as estimated from the 5 GHz flux.

The average spectral index (defined by $F_\nu \propto \nu^\alpha$), implied for the spectrum of UV Ceti is $\alpha = -0.26$. However, this becomes more steeply falling during the event B, where most of the extra flux emerges at 5GHz. The spectral index at the peak of the radio flare is $\alpha = -1.8$. This type of sharply falling spectrum is suggestive of gyrosynchrotron emission.

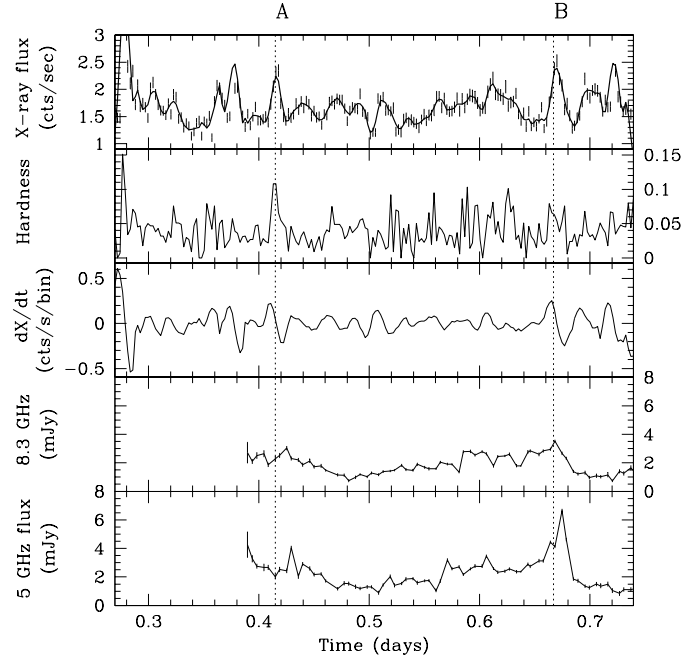


Fig. 7. Lightcurves for UV Ceti. From the top, the X-ray flux, hardness ratio, derivative of the X-ray flux, 8.3 GHz flux and 5 GHz flux. The time is in IAT days after IAT=0h on 07.07.2001

5.5. YZ CMi

The X-ray lightcurve of YZ CMi (Fig. 9) shows a period of quiescence followed by a series of flares towards the end of the observation. An increase in flux occurs at about 0.45 days, labelled A, and is followed by a higher plateau, which leads slowly into another increase just past 0.5 days (event B). Finally, a flare occurs just before the end of the observation at about 0.56 days (event C). The radio lightcurve shows a small flare-like event, at about 0.41 days, and possibly another small flare at 0.45 days which may correspond to event A. Neither of these flares was found to show any significant circular polarization. There is no clear counterpart to events B or C.

The energy budget calculation was performed for the flare labelled A. The X-ray flare radiates an estimated energy of 3×10^{31} erg. Event B appears very similar, with a more gradual and symmetric X-ray event preceded by a small radio spike. The energy budget calculation is very similar for this event as for event A, with the X-ray energy being approximately 3×10^{31} erg. Event C appears not to have a corresponding radio flare. A search of the high-resolution radio data also failed to uncover a counterpart.

5.6. Overall picture

In Figure 10 we plot the cross correlation of the radio lightcurves with the X-ray lightcurves for each of the stars. The lightcurves do not show strong correlations over their

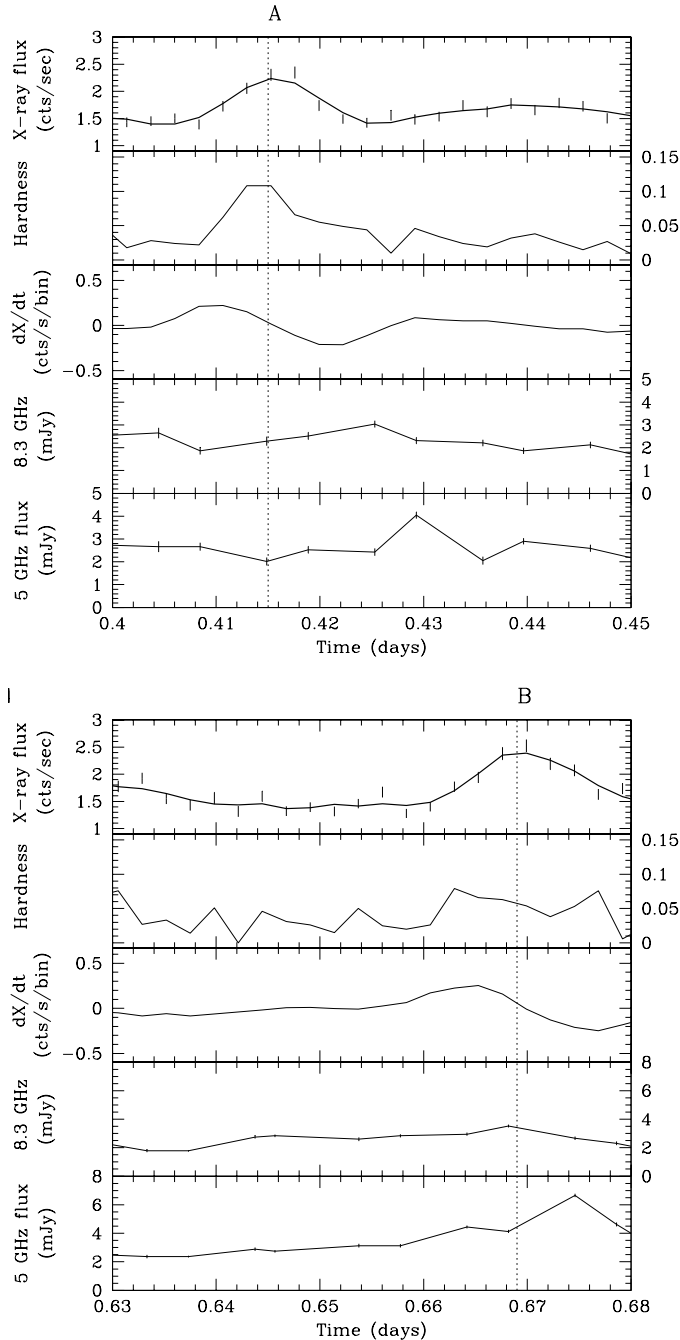


Fig. 8. Closeup of event A (top) and event B (bottom) for UV Cet

entire duration, with the exception of AU Mic which has a correlation coefficient of 0.72 at zero lag.

In the left-hand panel of Figure 11 we show the particle kinetic energy as estimated from the radio data plotted against the radiated X-ray energy for a total of ten events for which a plausible radio counterpart to an X-ray flare was observable. The particle kinetic energy is a function of the local magnetic field and the electron energy distribution power-law index, so it is necessary to choose fiducial values of these quantities in order to calculate a repre-

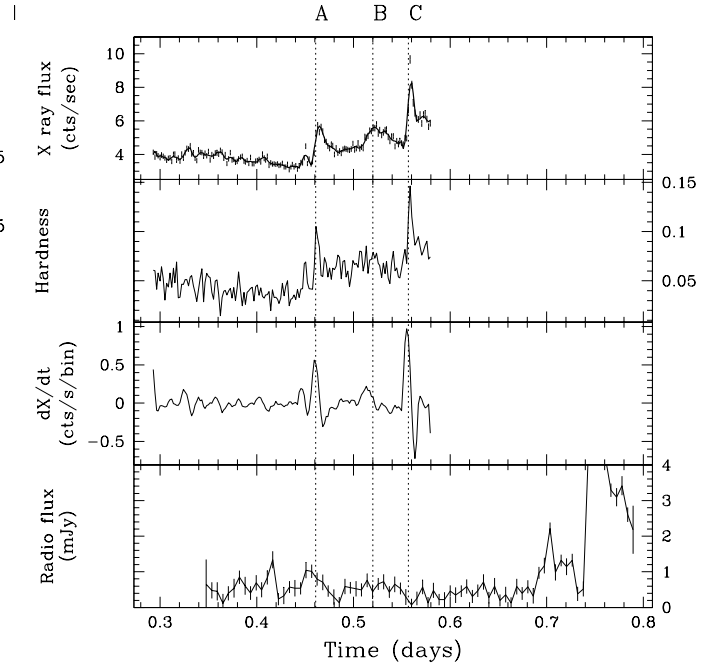


Fig. 9. Lightcurves for YZ CMi. The layout is the same as for previous cases for AD Leo, AU Mic and AT Mic. The time axis is labelled in days since 9.10.2000.

sentative energy. We have chosen $\log(B) = 1.5$, which is equivalent to $B = 31.6$ G, and $\delta = 3.0$, which results in total particle kinetic energies larger in every case than the radiated X-ray energy. The dependence of the estimated energy on the choice of values for B and δ can be estimated from the various contour plots. To decrease the inferred particle energy by one order of magnitude requires in each case an increase of approximately a factor of two in B , or alternatively a decrease in δ to around 2.3. A loose correlation between the two energies plotted in Fig. 11 is visible by eye. The Pearson correlation coefficient is 0.52. A non-parametric Kendall test reveals rank correlation with a significance at the 1.5σ level. The correlation is therefore not significant.

In the right-hand panel of Fig. 11 we show for each event the value of B implied if the available kinetic energy is equal to the radiated X-ray energy, for the case that $\delta = 3$. This is then the maximum value of B which is possible with that value of δ , and must underestimate the true value since the heating and X-ray emission process will not be 100% efficient. The straight line shows the relation $B \propto E_X^{-0.4}$, which would be expected if the observed radio flux were independent of the observed X-ray flux. No systematic deviation from this relation can be seen.

6. Conclusions

We have observed five flare stars simultaneously in X-rays with the *XMM-Newton* EPIC cameras and with the VLA.

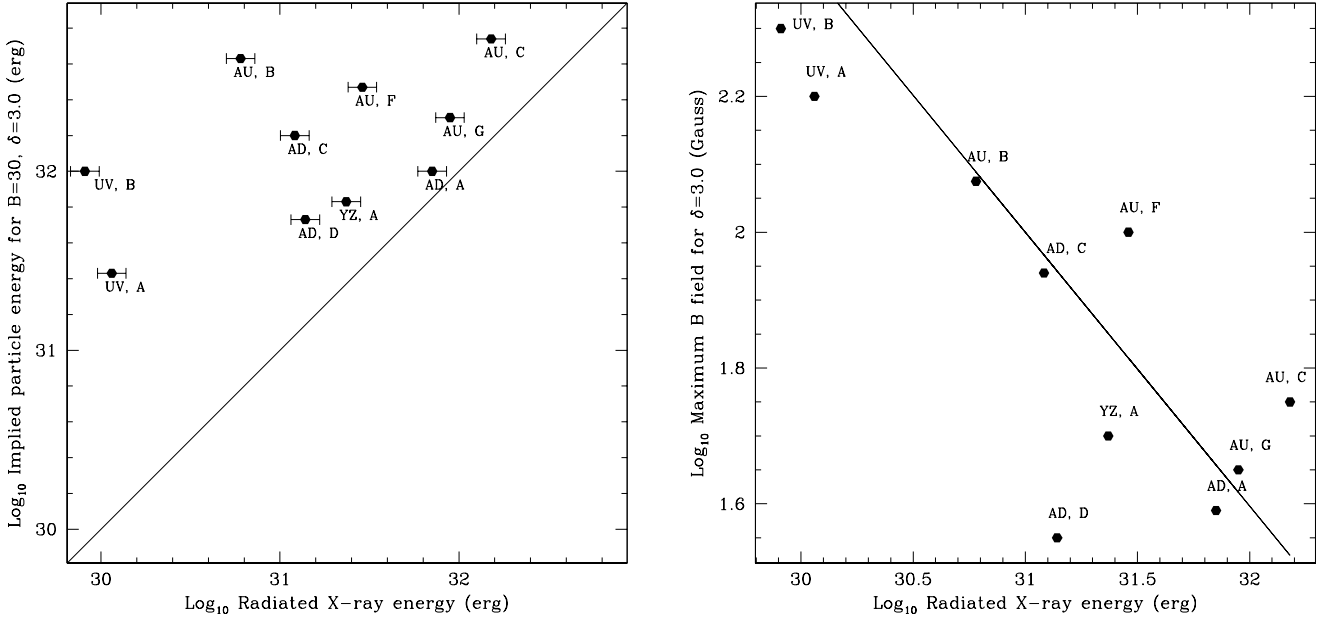


Fig. 11. Left: Comparison of radiated X-ray energy with inferred particle energy for ten events in which plausible radio counterparts to X-ray flares could be identified. Each point is labelled with the first two letters of the stars’ name and the identification letter of the flare in question. Right: The value of B for each of the ten events for which the particle kinetic energy matches the radiated X-ray energy for $\delta = 3.$ This is the maximum value of B possible with that assumption. The straight line shows the relation $B \propto E_X^{-0.4}$, which is expected in the event that the radio flux is uncorrelated with the X-ray flux. The events AD A, AD C, AU C and AU G are shown in detail in the various contour plots above.

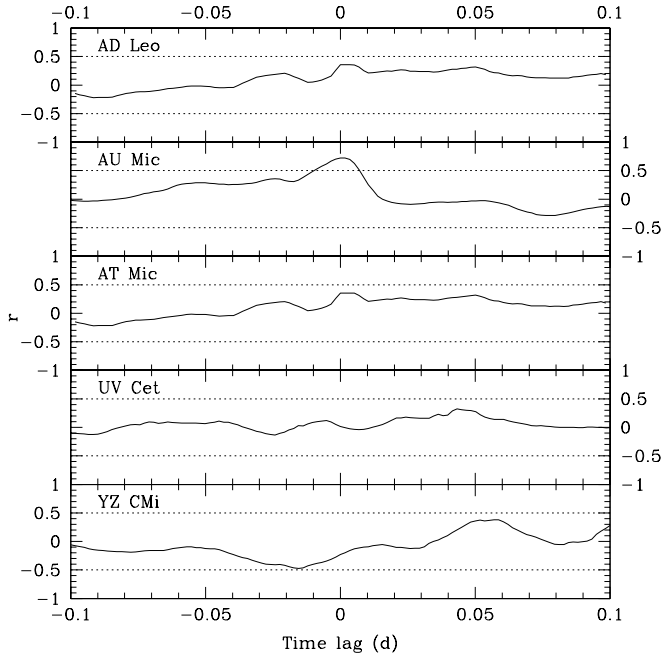


Fig. 10. Cross correlation of the X-ray and radio lightcurves for the five targets. Correlations of ± 0.5 are indicated with dotted lines. The overall lightcurves do not correlate well, with the exception of AU Mic which has a peak correlation of 0.72.

Comparisons of the behaviour at these two regimes can reveal relationships between the radio and X-ray emission which can often be interpreted in terms of standard models developed for solar flares. In particular, nearly-simultaneous radio and X-ray flares are suggestive of the Neupert effect, in which the same population of accelerated electrons is responsible for the synchrotron emission seen in radio, the heating of material which then emits in hard X-rays, and the evaporation of chromospheric material which then emits soft X-rays.

We identified a total of 17 large, distinct X-ray flares during the time periods when radio observations were also available. Of these, ten had possible counterparts in the radio lightcurve, and of these ten four showed good correlation between strong events in X-ray and strong events in the radio lightcurve. An energy budget calculation was performed for each of the ten cases, in which the total energy available from gyrosynchrotron emitting electrons was estimated for various values of magnetic field strength and power-law slope, and compared to the total energy radiated in X-rays. The radiated X-ray energy should be lower than the estimated available particle energy for the Neupert effect to be a viable hypothesis to explain the apparently related flare events. In all these cases the Neupert effect hypothesis was found to be credible on energy budget grounds. Of the ten correlated flares, AD Leo event C, AU Mic event C, AU Mic event G and UV Cet event B

show the strongest correlation between radio and X-ray behaviour, and must be the strongest candidates for a Neupert effect.

A few examples of radio flares with no X-ray counterpart were observed. One particularly strong example in the lightcurve of AD Leo was found to be highly circularly polarized, suggesting a coherent emission process and allowing the local magnetic field to be estimated based on the assumption of an electron-cyclotron maser as the source. The magnetic field strength suggested is of the order of kilogauss, which would then imply that the kinetic energy available to generate X-ray emission is very low.

Several examples of X-ray flares with no radio counterparts were also observed. Searches were made at high time resolution for evidence of very rapid continuous radio flaring, which might provide a heating mechanism, but evidence for this was not compelling. The lack of radio emission associated with some X-ray flares could be due to the emission being mostly synchrotron radiation from high energy electrons, which is emitted preferentially perpendicularly to the magnetic field lines.

The overall behaviour of the sources is complex, and while a convincing case can sometimes be built for causal connections between individual radio and X-ray events, there are also many cases where radio events are *not* related to any X-ray event, and vice versa. This then opens the possibility of coincidentally simultaneous or near-simultaneous flares which are not in fact related. We suggest that, for a causal connection to be considered likely, temporal coincidence alone cannot be a reliable indicator but must be combined with other tests, such as correlation of structure in the time-resolved flare lightcurves, and a clear demonstration that the X-ray-radio relationship is energetically plausible.

Acknowledgements. We thank the referee for providing insightful and careful comments which have helped us to improve the manuscript. This work is based on observations obtained with *XMM-Newton*, an ESA science mission with instruments and contributions directly funded by ESA Member States and the USA (NASA). The VLA is a facility of the National Radio Astronomy Observatory, which is operated by Associated Universities, Inc., under cooperative agreement with the National Science Foundation. This work has been funded in part by the Swiss National Science Foundation (grant 20-66875.01).

References

- Ambruster C. W., Sciortino S. & Golub L. 1987, ApJS 65, 273
 Andrews A. D., 1989, A&A 214, 220
 Audard M., Güdel M., Drake J. J. & Kashyap V. L., 2000, ApJ 541, 396
 Audard M., Güdel M. & Skinner S. L., 2003, ApJ 589, 983
 Balega I., Bonneau D. & Foy R., 1984, A&AS 57, 31
 Benz A.O., *Plasma Astrophysics*, second edition, Astrophysics and Space Science Library, Vol 279, Kluwer Academic Publishers, Dordrecht, 2002.
 Bromage G. E., Phillips K. J. H., Dufton P. L. & Kingston A. E. 1986, MNRAS 220, 1021
 Cully S. L., Fisher G. H., Abbott M. J. & Siegmund O. H. W., 1994, ApJ 435, 449
 Dennis B.R., 1988, Sol. Phys. 118, 49
 Dennis B.R. & Zarro D.M., 1993, Sol. Phys. 146, 177
 Dulk G.A., 1985, ARA&A 23, 169
 Dulk G.A. & Marsh, 1982, ApJ 259, 350
 Favata F., Micela G. & Reale F., 2000, A&A 354, 1021
 Güdel M. & Benz A. O. 1993, ApJ 405, L63
 Güdel M., Benz A. O., Schmitt J. H. M. M. & Skinner S. L., 1996, ApJ 471, 1002
 Güdel M., Audard, M., Smith, K.W., Behar E., Mewe R., 2002a, ApJ 577, 371
 Güdel M., Audard M., Skinner S.L., Horvath M. I., 2002b, ApJ 580, L73
 Güdel M., Audard M., Kashyap V. L., Drake J. J. & Guinan E. F., 2003, ApJ 582, 423
 Gunn A. G., Doyle J. G., Mathioudakis M., Houdebine E. R. & Avgoloupis S. 1994, A&A 285, 489
 Hawley S. L., Fisher G. H., Simon T., Cully S. L., Deustua S. E., et al. 1995, ApJ 453, 464
 Hawley S. L., Allred J. C., Johns-Krull C. M., Fisher G. H., Abbett W. P., et al., 2003, ApJ 597, 535
 Houdebine E. R. & Doyle J. G. 1994, A&A 289, 185
 Kashyap V. L., Drake J. J., Güdel M. & Audard M. 2002, ApJ 580, 1118
 Katsova M. M., Drake J. J. & Livshits M. A., 1999, ApJ 510, 986
 Krucker S. & Benz A. O., 1998, ApJ 501, L213
 Kundu M. R., Jackson P. D., White S. M. & Melozzi M., 1987, ApJ 312, 822
 Large M. I., Beasley A. J., Stewart R. T. & Vaughen A. E. 1989, Proc. Astron. Soc. Australia 8, 123
 Monsignori Fossi B. C., Landini M., del Zanna G. & Bowyer S., 1996, ApJ 466, 427
 Morris D. H., Mutel R. L., & Su B., 1990, ApJ 362, 299
 Nelson G. J., Robinson R. D., Slee O. B., Ashley M. C. B., Hyland A. R., et al. 1986, MNRAS 220, 91
 Neupert W.M., 1968, ApJ 153, L59
 Pagano I., Linsky J. L., Carkner L., Robinson R. D., Woodgate B. & Timothy G., 2000, ApJ 532, 497
 Pestalozzi M. R., Benz A. O., Conway J. E. & Güdel M., 2000, A&A 353, 569
 Raassen A. J. J., Mewe R., Audard M. & Güdel M. 2003, A&A 411, 509
 Robinson R. D., Carpenter K. G. & Percival J. W., 1999, ApJ 516, 916
 Robinson R. D., Linsky J. L., Woodgate B. E. & Timothy J. G. 2001, ApJ 554, 368
 Spiesman & Hawley, 1986, AJ 92, 664
 Stepanov A. V., Kliem B., Zaitsev V. V., Fürst E., Jessner A., et al. 2001, A&A 374, 1072
 van den Besselaar E.J.M., Raassen A. J. J., Mewe R., van der Meer R. L. J., Güdel M. & Audard M. 2003, A&A 411 587
 Vogt S.S., Penrod G.D. & Soderblom D.R., 1983, ApJ 269, 250